Geochemistry investigations of volcanic rocks in Salafchegan –Khorhe sheet with emphasize on Sr-Nd isotopic data

Farimah Ayati

1- Department of Geology, Payame Noor University, I.R. Iran.

* Corresponding Author: f.ayati@pnu.ac.ir

Received: 22 June 2014 / Accepted: 15 June 2015 / Published online: 18 June 2015

Abstract

Salafchegan-Khorhe volcanic rocks are exposed within Urumieh-Dokhtar magmatic belt. Different kinds of volcanic and subvolcanic rocks of calc-alkaline to alkaline character have been reported throughout this magmatic belt. Since, isotopic investigations are very useful for detection of magma petrogenesis and because no isotopic studies have been done in this area, so a geochemical and isotopic study was carried out for Salafchegan igneous rocks, Sw of Tehran, in order to constrain their petrogenesis and confirm that parental magma in this area, is similar to calc-alkaline magmas related to continental margin arc environments. The igneous rocks dominantly consist of andesite, diorite, quartz-diorite, tonalite, dacite-rhyodacite and granodiorite porphyries with calc-alkaline affinity. Harker diagram indicates that amphibole, biotite and plagioclase have played an important role during the crystallization of Salafchegan igneous rocks and proves the effect of fractional crystallization during magmatic evolution. These rocks are characterized by enrichment in light rare earth elements (LREE) and large ion lithophile elements (LILE) and depletion of HREE and HFSE and negative anomalies of Nb, Ti, Zr and P that indicated the formation of rocks in a subduction zone of active continental margin. The $^{87}Sr/^{86}Sr$ and $^{143}Nd/^{144}Nd$ isotopic ratios of the studied rocks are from 0.705201 to 0.707187 and 0.512508 to 0.512646 respectively. All of these samples are characterized by negative εNd values which can show the role of crustal contamination in their petrogenesis and also suggest the enrichment of the lithospheric mantle beneath this orogenic belt. The geochemical and Nd-Sr isotopic data demonstrate that fractional crystallization and assimilation have played an important role in magmatic evolution of this region.

Keywords: Crustal contamination, Subduction zone, Urumieh-dokhtar, Salafchegan-Khorhe.

1- Introduction

The studied area is associated with calc-alkaline volcanic- subvolcanic rocks in the Cenozoic Urumieh-dokhtar magmatic belt (UDMB). This belt extends north-west ward from Sahand volcano in Azarbaijan province to Bazman volcano in south east of Iran. This belt parallels the Zagros fold and thrust belt, northeast of the main thrust fault zone and an intervening longitudinal tectonic depression (Fig. 1). This belt was formed by subduction of the Arabian plate beneath Central Iran during the Alpine orogeny (Pourhosseini, 1982; Hezarkhani, 2002). Volcanism, plutonism and associated mineralization in the Urumieh Dokhtar magmatic belt are considered to be the result of subduction (e.g. Berberian and King, 1981) within the collisional Zagros belt. With the closure of Neo-Tethys ocean, the Afro-Arabian tectonic plate started to be subducted beneath south-central Iran, developing a NE-dipping subduction zone; relative plate motions at an incidence angle of about 45 degree were

responsible for oblique convergence and formation of collision–type subduction involving strike slip shear (Sokoutis *et al*., 2000; Mohajjel *et al*., 2003) from the late Cretaceous to the Paleocene. Post-Paleocene SW-vergent thrusting and strike slip faulting with resulting shortening, shearing and crustal thickening are consistent with a compressional regime. Extensive volcanic activity (Berberian and King, 1981) accompanied this compression.

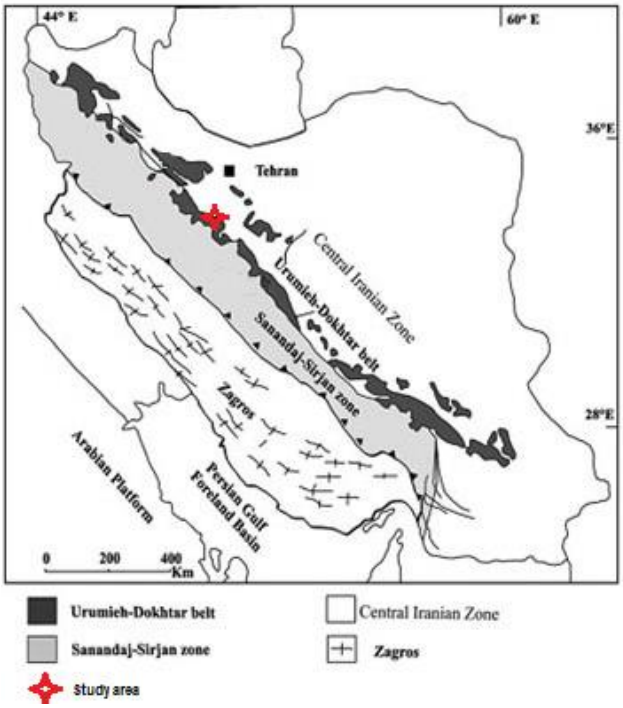

Figure 1) Index map showing the major geological-structural zones of Iran and location of the studied area (after Alavi, 1994; Mohajjel et.al, 2003).

After the compressive stage, extensional faults and localized relaxation "rifting" developed in several parts of the Iranian continental margins. Calc-alkaline granitoid magmatism of the UDMB is probably associated with this extensional episode (e.g. Alavi, 1994). In the early to middle Tertiary (Eocene to Miocene), a major episode of volcanism, plutonism and deformation occurred in the Urumieh Dokhtar magmatic belt. In the studied area, magmatism was initiated by eruption of Miocene volcanic to subvolcanic rocks which continued to Pliocene time. The composition of these rocks varied from basaltic andesite to dacite. To date no Sr-Nd isotopic studies have been undertaken on these igneous rocks in Salafchegan area. In order to better constrain the origin of these rocks, we present combined geochemical and Nd-Sr isotopic data for these Miocene Pliocene igneous rocks and discuss their petrogenesis.

2- Geological setting

The UDMB which is characterized by a linear magmatic arc is part of the Alpine-Himalayan orogenic and metallogenic belt that extends from the Eastern Anatolian fault in eastern Turkey to the Oman line in southern Iran, within a distance over 2000 km (Alavi 1994; Zarasvandi *et al*., 2005). The calc-alkaline magmatic activity in this arc was started in the Eocene and continued to the Quaternary. The younger volcanic activity is characterized by the alkaline rocks in relation to the tectono-magmatic processes (Jamali *et al*., 2010). The Oligo-Miocene magmatic rocks from diorite to granite and intermediate to acid flows and pyroclastics are widespread in the UDMB.

The studied area is located at the SW of Tehran. Studied igneous rocks show small to large outcrops in 1/100000 geological map of Salafchegan-Khorhe (50° 14′ to 50° 30 ′ E - 34° 15′ to 34° 30 ′ N). The oldest rocks exposed in this area are a sequence of Miocene red marl with intercalations of sandstone, conglomerate and gypsum. This sequence is intruded by the Miocene-Pliocene bodies of basaltic andesite lava flow, andesite, diorite, quartz-diorite, tonalite, dacite-rhyodacite and granodiorite porphyries with calc alkaline affinity and by numerous calc-alkaline basaltic andesite and andesitic dykes (Fig. 2). These rocks have a simple mineralogical composition. The porphyritic rocks are composed mainly of quartz, plagioclase, mica, amphibole and rarely pyroxene phenocrysts. Andesite represents the main lithology of the studied area and is present in the whole studied zone**.** One part of the studied area were subjected to intense hydrothermal alteration, several stages of

hydrothermal alteration and associated mineralization have produced new minerals, created new textural relationships and in many cases, obliterated the primary character of the rocks. This mineralization part which is described in detail by (Ayati *et al*., 2008, 2013) and is not the central argument in this article, called Dalli, and is a copper porphyry system. There are three mineralized porphyry centre at this area which lie within a NE trending corridor of altered Oligo-Miocene intrusives. Almost all intrusive units contain the same assemblge of minerals: plagioclase, hornbelende (typically altered to biotite and / or chlorite), biotite, quartz and K-feldspar. They are porphyritic and suggest a shallow level of emplacement (Ayati *et al*., 2008, 2013). Three types of hypogen alterations were recognized at this area, such as potassic, phyllic and propylitic. Mineralization and hydrothermal alteration are superimposed onto Neogene volcanic-plutonic rocks and neighbouring country rocks. The $^{40}Ar/^{39}Ar$ age data indicates a minimum emplacement age of ~21 Ma for a potassically altered porphyritic diorite that hostthe porphyry system (Ayati *et al*., 2013).

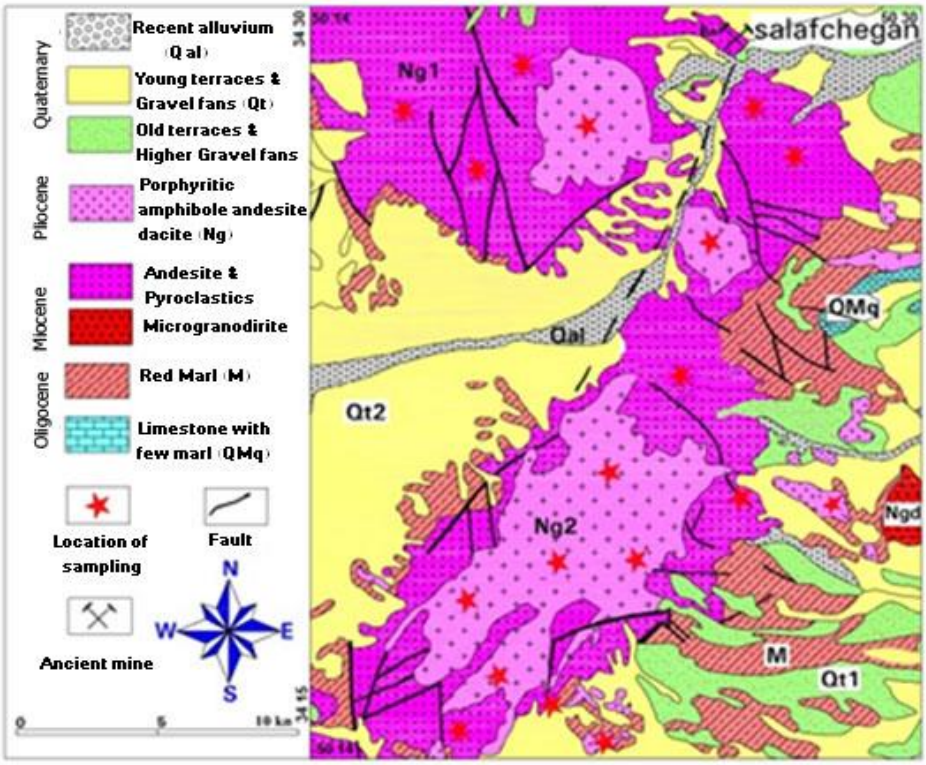

Figure 2) Simplified regional geological map of the studied area (Modified from Geological Survey of Iran (2000; Ayati et al., 2010).

3- Petrography

The igneous rocks of the studied area were sampled for the freshest material available. Brief petrographical descriptions for these rocks are given below: They are porphyritic contain phenocrysts of plagioclase, biotite, hornblende and sometimes pyroxene in a fine grained to microcrystalline matrix which are mostly euhedral to subhedral. Plagioclase present as the most common phenocryst phase in the andesitic and dacitic volcanic rocks of the study area. The groundmass consists mainly of quartz and plagioclase. The Compositions ranges of plagioclases are from andesine to oligoclase (An_{4-69}) in the core and sometimes to albite at the rim. They sometimes show sieve texture and have normally to oscillatory zoning as well as sometimes altered to sericite, chlorite and opaque.

Amphibole is the most abundant mafic mineral in igneous units. Amphiboles from barren rocks are relatively iron rich and display only minor

composition variation. In contrast, amphiboles from mineralizing rocks span the range from magnesio-hornblende to actinolite. Euhedral to subhedral amphiboles displays brown to pale green pleochroism of variable intensity. It displays a large compositional range, varying from magnesiohastingsite to tschermakite to magnesiohornblende, in the differentiation sequence from basaltic andesite to dacite with $Mg/(Mg+Fe_{tot})$ ratios ranging from 0.59 to 0.79. Amphiboles are characteristically ferric iron-rich, with $Fe^{3+}/(Fe^{3+}+Fe^{2+})$ ratios ranging between 0.00 and 0.78 reflecting the oxidized nature of the melt. Calcic-amphibole is a ubiquitous phase in all of the igneous rocks in this area; it occurs as phenocryst or as a groundmass phase.

Biotite phenocrysts are brown in color, Fe to Mg-enriched and euhedral to subhedral and sometimes have been altered to chlorite and sericite. Pale brown to greenish brown, more Mg- riched biotite formed small ragged crystals are interpreted to be of hydrothermal origin. Primary biotite which is distinguished from secondary biotite by shape and the fact that secondary biotite has less developed cleavage and is green to pale brown in color. Biotite phenocrysts have low to moderate Al atoms per formula unit contents and Fe/(Fe+Mg) ratios in a narrow range from 0.34 to 0.37. These parameters reflect relatively oxidizing condition during late stage crystallization, including possible crustal contamination. Relatively high X_{Mg} values both in biotite (mean = 0.64) and amphibole (mean = 0.66) are common in subvolcanic rocks showing that the magma was saturated with water during its emplacement (Ayati *et al*., 2013).

Clinopyroxene is present in the basaltic andesites and andesites. It is often altered (chloritization and/or uralitization). Accessory minerals include zircon, apatite and sphene which occur randomly. In the mineralized area opaque minerals include dominantly pyrite, chalcopyrite and magnetite.

4- Methodology

Compilation of satellite images, geological maps and reports and detailed geological mapping of the area were used. About 100 rock samples were collected for lithochemistry, described petrographically and about sixty rock samples were analyzed for major, trace and rare earth elements by Actlabs laboratory in Canada, Amdel laboratory in Australia and at Laboratories de Géochimie Isotopique et Géodynamique Chimique, Université Libre de Bruxellesusing XRF and inductively coupled plasma mass spectrometry (ICP-MS). Whole-rock X-ray fluorescence (XRF) spectrometric analyses of major elements and of Cr were made on fused glass discs at the University of Lie`ge (Collectif de Géochimie instrumental). Some trace elements (Ni, Cu, Zn, V and Sr) were measured by X-ray fluorescence spectrometry on pressed powder pellets (Bologne and Duchesne, 1991). Other trace elements (Rb, Cs, Ba, Zr, Nb, U, Th, Pb, Y and the REEs) were analyzed by ICP-MS, also at the ‘‘Collectif de Géochimie instrumentale’’ Brussels University, using the analytical procedure described by Vander Auwera *et al*. (1998) and detailed in Féménias *et al*. (2003). The whole-rock geochemical data are reported in Table 1. The 24 samples were selected for $^{87}Sr/^{86}Sr$ and 6 samples for $^{143}Nd/^{144}Nd$ isotopic ratios determination, corrected to the 25 Ma ages of the studied igneous rocks. These samples were analyzed at Laboratoire de Géochimie Isotopique et Géodynamique Chimique, Université Libre de Bruxelles. The results are presented in Table 2.

**Table 1) Whole-rock major (wt. %), trace (ppm) and rare earth elements data for representative samples of Salafchegan igneous rocks.*

	S-Kh1	**S-kh2**	**S-Kh7**	**S-Kh 9**	**S-Kh 10**	**S-Kh 12**	**S-Kh 13**	**S-Kh 15**	**sample17***	**sample19***	**sample20***
Wt%	volcanic	volcanic	volcanic	volcanic	volcanic	volcanic	volcanic	volcanic	volcanic	volcanic	subvolcanic
SiO_2	61.4	60.2	62.7	61.9	63.5	60.6	56.7	63.5	63.19	60.03	63.47
TiO_2	0.55	0.65	0.53	0.54	0.52	0.58	0.66	0.5	0.567	0.653	0.586
Al_2O_3	16	16.3	16.2	16.3	16.5	16.4	15.5	15.9	15.9	15.89	17.04
Fe_2O_3	5.4	5.9	5.4	5.9	5.1	5.6	7.4	5.6	5.3	6.05	4.97
MnO	0.12	0.14	0.09	0.09	0.11	0.14	0.14	0.07	0.112	0.191	0.043
MgO	2.4	3.2	2	2.2	2	2.5	4.3	1.7	2.04	2.33	2.27
CaO	5.2	4.9	4.5	4.5	4.1	5.6	5.7	4.3	4.67	5.65	2.57
Na_2O	4.2	3.8	4.4	4.2	4	3.8	4.1	4.3	3.43	3.47	3.41
K_2O	2.3	2.3	2.7	2.5	2.6	2.1	2.2	3	2.59	2.38	2.34
P_2O_5	0.17	0.16	0.17	0.17	0.16	0.17	0.15	0.16	0.17	0.16	0.17
LOI	1.4	2.3	1.1	1.7	1.4	2.3	2.4	1.3	1.65	2.69	2.58
Tot	99.14	99.85	99.79	100	99.99	99.79	99.25	100.33	99.62	99.49	99.44
Mg#	63.78	68.24	59.70	59.64	61.07	63.88	69.72	54.6	60.62	60.64	64.63
A/CNK	0.849	0.923	0.882	0.915	0.978	0.876	0.794	0.875	0.938	0.855	1.328
A/NK	1.702	1.865	1.593	1.695	1.755	1.923	1.697	1.539	1.881	1.916	2.091
Na_2O/K_2O	1.83	1.65	1.63	1.68	1.54	1.81	1.86	1.43	1.32	1.46	1.46
ppm											
Li	34.6	50.2	3.6	11.4	5.9	16.3	8	4.4	___	___	___
Be	1.7	1.5	1.5	1.6	1.6	1.5	1.2	1.5	<2	<2	<2
S	110	90	90	130	0	70	80	0	0.02	0.012	0.004
Sc	12	15	9	12	10	12	20	8	9.8	14.2	10.5
V	126	143	96	130	99	125	163	90	106	131	109
Cr	13	18	13	10	7	10	69	11	19.1	36.5	15.1
Co	14.1	16.4	11.9	10.4	22.5	10.3	16.2	16.8	11.2	16.4	20.3
Ni	10	13	10	9	8	10	28	10	10	12	14
Cu	33.5	116	660	22.7	1200	16.3	1130	321	16	53	2740
Zn	87	263	64.2	72.6	130	67.6	187	66.6	62	301	92
As	8.7	8.1	2.5	3.3	4	19.7	3.8	0	5	20	3
Rb	84.9	81.5	55.1	53	46.05	56.3	82.7	40.2	72	81	71
Sr	536	520	474	437	438	560	451	488	574	424	362
Y	14.9	15	14	14	22	14	15.7	7.87	19.5	17	19
Zr	142.2	127.3	133.3	133.6	133	130	128	135.3	115	127	143
Nb	15.3	6.8	9.6	6.2	8.01	6	10.3	10.9	5.7	6.3	7

** (Ayati et al., 2013)*

Table 1) Continued.

	sample21*	**sample 22***	**S-Kh23**	**sample 24***	**sample 26***	**S-Kh 27**	**S-Kh 28**	**S-Kh 29**	**S-Kh 30**	**S-Kh 31**	**S-Kh 32**
Wt%	subvolcanic	subvolcanic	subvolcanic	subvolcanic	volcanic	volcanic	volcanic	volcanic	volcanic	volcanic	volcanic
SiO_2	63.51	66.45	62.9	62.47	61.4	56.1	53.9	54.4	54.9	53.2	54.8
TiO_2	0.513	0.436	0.52	0.533	0.57	0.71	1.0	1.0	1.0	1.0	0.9
Al_2O_3	16.04	15.61	16.2	16.28	15.85	16.6	18.2	17.9	19.1	18.2	19.1
Fe_2O_3	5.01	4.43	5	5.04	5.6	7.6	9.8	9.1	8.5	9.1	8.6
MnO	0.101	0.077	0.12	0.108	0.096	0.14	0.1	0.1	0.1	0.1	0.1
MgO	2.28	1.56	2.2	2.11	2.17	5.4	3.5	3.9	3.2	4.3	3.3
CaO	4.65	3.92	4.5	4.33	4.96	6.9	8.4	8.5	8.0	6.9	8.3
Na_2O	3.45	3.8	4.2	3.66	3.27	3.1	3.1	2.9	3.0	3.2	3.0
K_2O	2.26	2.98	2.4	2.41	2.48	1.3	1.3	1.1	1.3	1.4	1.0
P_2O_5	0.15	0.13	0.17	0.16	0.16	0.15	0.1	0.1	0.2	0.2	0.2
LOI	2.16	0.87	1.3	1.7	2.51	2.1	1.28	1.75	1.77	2.86	1.33
Tot	100.1	100.2	99.51	98.81	99.06	100.10	101.73	100.84	100.95	100.46	100.51
Mg#	64.54	58.48	63.55	62.61	60.78	73.97	58.62	63.08	59.98	65.35	60.39
A/CNK	0.966	0.939	0.916	0.985	0.927	0.870	0.834	0.841	0.917	0.889	0.907
A/NK	1.973	1.646	1.704	1.885	1.964	2.550	2.825	3.035	3.028	2.786	3.183
Na_2O/K_2O	1.53	1.28	1.75	1.52	1.32	2.38	2.44	2.59	2.35	2.34	3.12
ppm											
Li	___	___	7	___	___	12.4	___	___	___	___	___
Be	<2	<2	1.6	<2	<2	0.8	___	___	___	___	___
S	0.016	0.009	140	0.007	0.018	70	175	___	___	___	___
Sc	9.62	7.73	10	10.3	10.7	22	___	___	___	___	___
V	90	70	105	97	107	180	280	270	193	248	176
Cr	32.8	26.3	7	25.6	19.6	61	89	90	89	61	71
Co	8.4	7.9	10.6	10.3	9	17.2	27.3	30.2	17.7	30.4	24.7
Ni	14	10	8	10	9	32	1.6	1.2		1.9	
Cu	210	354	135	68	4	96.1	19.5	70.3	37.9	51.0	25.9
Zn	55	52	61	55	63	98.5	89.3	87.4	77.5	77.8	72.3
As	13	3	2.6	5	13	1.7	___	___	___	___	___
Rb	59	90	82.5	76	61	30.2	34.8	34.5	30.4	24.9	22.3
Sr	411	383	439	396	460	385	342.0	344.9	331.7	395.2	321.8
Y	18	15	14.5	17	17	12.5	23.9	22.9	26.1	25.2	25.7
Zr	141	123	120	133	134	94	115.1	112.9	105.2	107.4	104.0
Nb	7.1	7.2	6.1	6.8	6.6	3.7	4.3	4.4	4.7	4.1	5.5

Table 1) Continued.

	S-Kh1	**S-kh2**	**S-Kh7**	**S-Kh 9**	**S-Kh 10**	**S-Kh 12**	**S-Kh 13**	**S-Kh 15**	**sample 17***	**sample 19***	**sample20***
ppm	volcanic	volcanic	volcanic	volcanic	volcanic	volcanic	volcanic	volcanic	volcanic	volcanic	subvolcanic
Mo	1.3	1.3	1.4	1.7	2.6	0.8	2.9	4.7	< 2	< 2	< 2
Ag	0.87	1.14	0.69	1.02	0.45	1.16	2.13	1.88	< 0.5	0.6	0.6
Cd	0.6	0.6	0.4	0.2	0.2	0.2	0.5	0.3	0.6	3.5	0.6
Sn	2.5	4.3	0.6	4.8	0	3.1	3.1	2.7	1	2	2
Sb	0.7	0.6	0.4	0.4	0.5	2.7	1	1	0.4	1.6	0.9
Te	1.6	1.6	0.6	1.6	0	1.6	1.3	2.6	-----	-------	------
Cs	1.9	2.2	0.5	0.7	1.7	0.8	1.1	0.9	------	2.7	3.5
Ba	848	818	793	1130	912	926	631	850	907	807	894
La	34	32	30	30	34	33	25	27	29	29.3	36.5
Ce	54.5	52.4	40.9	52.2	56.3	58.6	46.4	33.2	48.9	49.2	60
Pr	5.92	5.8	3.57	5.48	6.76	6.13	6.47	5.56	4.96	5.15	6.26
Nd	31	30.9	18.9	27.4	24.5	30.9	35.4	21.8	17.9	18.9	22.5
Sm	3.86	3.91	2.95	3.54	4.65	3.92	4.52	5.23	3.21	3.56	3.98
Eu	1.21	1.17	1.04	1.26	1.6	1.26	1.29	1.49	0.828	0.979	1.09
Gd	3.47	3.48	5.12	3.12	4.5	3.48	3.96	3.6	2.64	3.16	3.26
Tb	0.56	0.57	0.62	0.52	0.61	0.55	0.61	0.56	0.41	0.49	0.51
Dy	3.22	3.23	3.5	3.07	3.45	3.15	3.44	3.48	2.3	2.8	2.89
Ho	0.62	0.64	0.7	0.58	0.66	0.6	0.61	0.88	0.75	0.58	0.58
Er	1.92	1.94	2.58	1.78	2.08	1.8	2.19	1.23	1.38	1.67	1.75
Tm	0.28	0.27	0.33	0.25	0.27	0.25	0.29	34	0.34	0.259	0.274
Yb	1.86	1.87	2.13	1.62	1.63	1.64	1.51	1.02	1.02	1.77	1.85
Lu	0.28	0.28	0.29	0.23	0.51	0.24	0.21	0.4	0.243	0.289	0.304
W	2.9	2.9	0.27	3.2	0.28	3.1	2.6	6.4	< 1	< 1	< 1
Tl	0.8	0.8	0.5	1	0.6	0.5	1.1	5	0.9	0.81	0.84
Pb	74.2	215	30.1	52.5	19.85	18.8	38.6	36.5	19	600	43
Bi	0.1	0.3	0.5	0.2	0.4	0.2	1	7.3	0.2	0.4	0.7
Th	15.5	14.5	13.4	14.4	20.1	15.5	9.46	12.7	17.6	17.7	20.9
U	4.48	3.96	2.48	4.06	3.52	4.91	2.31	3.48	3.57	5.64	3.58

Table 1) Continued.

	sample 21*	**sample 22***	**S-Kh 23**	**sample 24***	**sample 26***	**S-Kh 27**	**S-Kh 28**	**S-Kh 29**	**S-Kh 30**	**S-Kh 31**	**S-Kh 32**
ppm	subvolcanic	subvolcanic	subvolcanic	subvolcanic	volcanic	volcanic	volcanic	volcanic	volcanic	volcanic	volcanic
Mo	< 2	< 2	0.5	< 2	< 2	1	___	___	___	___	___
Ag	< 0.5	< 0.5	1.3	< 0.5	< 0.5	1.23	___	___	___	___	___
Cd	< 0.5	< 0.5	0.2	< 0.5	< 0.5	0.2	___	___	___	___	___
Sn	2	2	0	1	2	0	___	___	___	___	___
Sb	1.7	< 0.1	0.2	< 0.1	1.2	3.1	___	___	___	___	___
Te	___	___	1.6	___	___	1.8	___	___	___	___	___
Cs	2.1	0.8	0.6	0.6	0.8	0.3	___	___	___	___	___
Ba	785	936	851	832	1197	305	343	285	308	338	284
La	26.7	32.6	37	34.4	33.1	14	___	___	16	___	___
Ce	47.1	52.4	63.5	57.9	56	32.8	44	36	46	42	44
Pr	5.15	5.28	6.41	6.06	5.89	3.7	___	___	4.3	___	___
Nd	19.6	18.9	33.1	22.3	21.8	20.8	___	___	21	___	___
Sm	3.75	3.34	4.01	4.05	3.99	3.42	___	___	3.2	___	___
Eu	0.975	0.874	1.19	1.03	1.09	0.96	___	___	0.97	___	___
Gd	3.22	2.72	3.35	3.25	3.31	3.32	___	___	3.38	___	___
Tb	0.5	0.41	0.56	0.51	0.5	0.53	___	___	0.56	___	___
Dy	2.85	2.43	3.03	2.92	2.87	2.86	___	___	2.8	___	___
Ho	0.58	0.5	0.58	0.6	0.58	0.53	___	___	0.58	___	___
Er	1.73	1.48	1.77	1.74	1.69	1.49	___	___	1.78	___	___
Tm	0.269	0.231	0.26	0.269	0.261	0.19	___	___	0.24	___	___
Yb	1.83	1.6	1.68	1.83	1.82	1.21	___	___	1.19	___	___
Lu	0.305	0.258	0.24	0.3	0.297	0.73	___	___	0.7	___	___
W	< 1	< 1	1.7	< 1	< 1	0.17	___	___	___	___	___
Tl	0.55	0.55	0.7	0.51	0.83	0.2	___	___	___	___	___
Pb	15	14	20.4	19	13	20.9	___	___	___	___	___
Bi	0.6	0.2	0	0.2	1	0.6	___	___	___	___	___
Th	16.3	26	17	19.4	19.9	2.19	8.1	8.4	11.8	5.1	7.3
U	4.42	4.66	3.55	4.38	6.13	0.51	5.0	3.4	2.1	1.7	3.9

Table 1) Continued.

	S-Kh1	**S-kh2**	**S-Kh7**	**S-Kh 9**	**S-Kh 10**	**S-Kh 12**	**S-Kh 13**	**S-Kh 15**	**sample 17***	**sample 19***	**sample20***
∑ REE	142.7	138.46	112.63	131.05	141.52	145.52	131.9	139.45	113.881	118.107	141.748
La/Yb	18.28	17.11	14.08	18.52	20.86	20.12	16.56	26.47	28.43	16.55	19.73
Sr/Y	35.97	34.67	33.86	31.21	19.95	40.00	28.73	62.01	29.44	3.34	2.53
(La/Lu)n	12.61	11.87	10.74	13.55	6.92	14.28	12.36	7.01	12.39	10.53	12.47
(La/Yb)n	12.32	11.53	9.49	12.48	14.06	13.56	11.16	17.84	19.16	11.16	13.30
(La/Sm)n	5.54	5.15	6.40	5.33	4.60	5.29	3.48	3.25	5.68	5.18	5.77
(Ce/Yb)n	7.58	7.25	4.97	8.34	8.94	9.24	7.95	8.42	12.40	7.19	8.39
(Gd/Yb)n	1.51	1.51	1.95	1.56	2.23	1.72	2.12	2.86	2.09	1.45	1.43
Ce/Ce*	0.93	0.93	0.96	0.98	0.90	1.00	0.88	0.66	0.99	0.97	0.96
Eu/Eu*	1.01	0.97	0.82	1.16	1.07	1.04	0.93	1.05	0.87	0.89	0.92

	sample 21*	**sample 22***	**S-Kh23**	**sample 24***	**sample 26***	**S-Kh 27**	**S-Kh 28**	**S-Kh 29**	**S-Kh 30**	**S-Kh 31**	**S-Kh 32**
∑ REE	114.559	123.023	156.68	137.159	133.198	86.54	43.86	36.00	102.72	41.51	43.91
La/Yb	14.59	20.38	22.02	18.80	18.19	11.57	___	___	13.45	___	___
Sr/Y	2.91	3.11	30.28	2.98	3.43	30.80	14.31	15.07	12.71	15.67	12.50
(La/Lu)n	9.09	13.12	16.01	11.91	11.57	1.99	___	___	2.37	___	___
(La/Yb)n	9.83	13.73	14.84	12.67	12.26	7.80	___	___	9.06	___	___
(La/Sm)n	4.48	6.14	5.80	5.34	5.22	2.57	___	___	3.14	___	___
(Ce/Yb)n	6.66	8.47	9.78	8.18	7.96	7.01	___	___	___	___	___
(Gd/Yb)n	1.42	1.38	1.61	1.44	1.47	2.22	___	___	___	___	___
Ce/Ce*	0.97	0.97	1.00	0.97	0.97	1.10	___	___	1.34	___	___
Eu/Eu*	0.90	0.89	0.99	0.87	0.92	0.86	0.88	0.99	0.87	0.85	0.91

Table 2) Sr-Nd isotopic analysis of Salafchegan-Khorhe igneous rocks.

samples	andesite	andesite	andesite	andesite	andesite	andesite	andesite	andesite	andesite	andesite	andesite	andesite	andesite
Sr	401.6903	543.392	431.1491	326.6798	468.0672	411.7077	485.9637	516.6	352.0376	392.6003	487.8313	178.4	467.9235
Nd	-----	-----	-----	20.8	30.9	18.7	21.6	-----	-----	-----	-----	-----	-----
$^{87}Sr/^{86}Sr$	0.707099	0.707184	0.706874	0.706253	0.706817	0.706251	0.706942	0.706913	0.706857	0.706028	0.706477	0.707114	0.706673
$^{87}Sr/^{86}Sr_i$	0.706894	0.707012	0.706728	0.706243	0.706709	0.706196	0.706889	0.706778	0.706844	0.705967	0.706427	0.706882	0.706536
$^{143}Nd/^{144}Nd$	-----	-----	-----	0.512566	0.512508	0.512597	0.512529	-----	-----	-----	-----	-----	-----
$^{143}Nd/^{144}Nd_i$	-----	-----	-----	0.512566	0.512508	0.512596	0.512528	-----	-----	-----	-----	-----	-----

samples	andesite	andesite	andesite	dacite	dacite	dacite	basaltic andesite	basaltic andesite	basaltic andesite	basaltic andesite	basaltic andesite
Sr	459.8212	539.1789	371.5415	377.8806	402.6305	366.8884	321.7745	395.2289	331.6813	341.9847	344.9259
Nd	-----	-----	-----	33.1	-----	-----	20.7	-----	-----	-----	-----
$^{87}Sr/^{86}Sr$	0.707187	0.707151	0.705808	0.707001	0.706953	0.706928	0.705618	0.705708	0.705842	0.705334	0.705201
$^{87}Sr/^{86}Sr_i$	0.706996	0.707008	0.705725	0.706798	0.706788	0.706686	0.705547	0.705643	0.705748	0.705229	0.705098
$^{143}Nd/^{144}Nd$	-----	-----	-----	0.512549	-----	-----	0.512646	-----	-----	-----	-----
$^{143}Nd/^{144}Nd_i$	-----	-----	-----	0.512549	-----	-----	0.512646	-----	-----	-----	-----

5- Discussion

5.1- Major and trace element geochemistry

Representative samples of whole rock of Salafchegan–Khorhe sheet were analyzed for major and trace element compositions. In the mineralized area (Dalli)–which as mentioned above, this article doesn't not focus on it- sometimes hydrothermal alteration affected some of the rock units and caused re-distribution/ mobilization of the alkali elements (e.g., K and Na) and process in some rock types. Based on Wang *et al*., 2006, the HFSE, REE, Th and transition elements are immobile during the most intense hydrothermal alteration (e.g. Zhou,1999; Hawkesworth *et al*., 1997). Mg is thought to be easily transported in solution and its content will be changed by alteration in some mafic rocks containing olivine and pyroxene, but it tends to be immobile and will not be greatly affected by alteration in intermediate–acid igneous rocks due to the lack of olivine and pyroxene (e.g., Zhou, 1999). In addition, some major elements such as Ti, P, Al, Fe and Mn are not readily transported by hydrothermal alteration (e.g. Zhou, 1999), but Ca, Na, K and the large ion lithophile elements (e.g. Sr, Ba and Rb) are generally mobile (Smith and Smith, 1976). The Al_2O_3, Fe_2O_3, MgO, TiO_2, P_2O_5 and Th contents of the Salafchegan igneous rocks show no obvious variation with increasing LOI (not shown) indicating that their contents have probably not been changed by alteration. This is true to some extent in the case of Na_2O and K_2O.

In the classification diagram of middlemost (1994), these igneous rocks, plot in the fields of basaltic andesite, andesite (diorite porphyry) and dacite (granodiorite) (Fig. 3) and defined as andesite and rhyodacite/dacite (or intrusive equivalents) using the Zr/TiO_2 versus SiO_2 diagram of Winchester and Floyd (1977). Their composition spans from medium to high K-field on the classification diagram of Peccerilo and Taylor (1976). The magma in this area is clearly sub-alkaline with a clear calc-alkaline affinity. All samples are related to the same magmatic series. The composition of igneous rocks is metaluminous and the ratio of the molecular A/CNK of these rocks is in 0.8-1.3 interval of A/CNK, hence they are of I-Type in the concept of Chappel and White (1974).

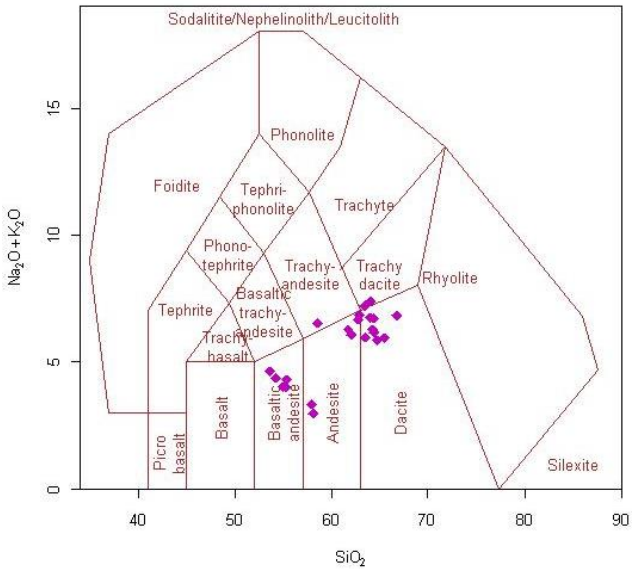

Figure 3) Classification of the analyzed rocks in the SiO_2 (wt %) versus Na_2O+K_2O diagram (after Middlemost,1994).

Trends of increasing alkalis (Na and K) with increasing SiO_2 are also consistent with such fractionation (crystallization of progressively more sodic plagioclase and K-feldespar too), we should consider the effects of potassic and sodic alteration, hydrothermal alteration characterized by secondary biotite and K-feldspar especially in the mineralized area.The plot of major and trace element of study rocks vs. SiO_2 (as an index of fractionation) in the Harker diagram, indicated that TiO_2, Al_2O_3, Fe_2O_3, MgO and CaO decrease with increasing SiO_2 (Fig. 4). Possibly such trends are consistent with fractionation of the observed phenocryst phases from a basaltic andesite as a parental magma. In fact, this type of variation shows that Fe- and Mg-rich rock-forming minerals, including amphibole and dark mica as well as plagioclase have played an important role during the crystallization of volcanic- subvolcanic rocks

and indicates the effect of fractional crystallization during magmatic evolution.

Trace and REE contents of these igneous rocks have been normalized to primitive mantle (Sun and McDonough, 1989) and chondrite (Boynton, 1984). In the primitive mantle-normalized multi-element variation diagram, these rocks show positive anomalies in Th, K and Pb and negative anomalies in Nb, P, Ti and Zr. Strong negative anomalies in Nb and Ti and positive anomaly in Pb are evidences of calc-alkaline arc-related magmas in worldwide (e.g., Gill, 1981; Pearce, 1982; Pearce and Peate, 1995) (Figs. 5a,b). In this diagram, all of the samples show typical subduction-related signatures. They are enriched in LILE (e.g., Ba, Rb, Sr and K) with respect to HREE (i.e., Yb and Lu) and HFSE (i.e., Nb, Ti and Zr).

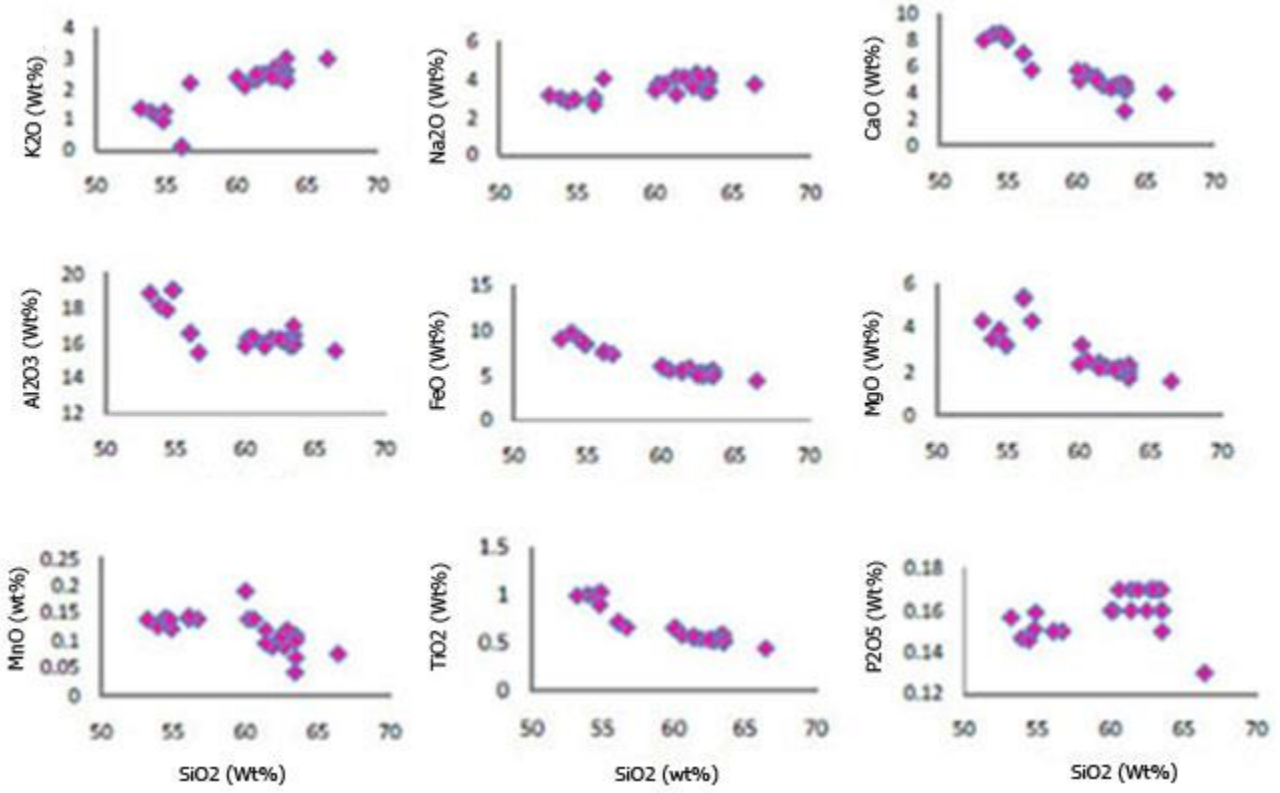

Figure 4) Variation diagrams for selected major oxides (wt %) versus SiO_2 (wt %) in the studied area volcanic- subvolcanic rocks.

All of the volcanic-subvolcanic rocks have similar distributions on chondorite-normalized spider diagram. This diagram shows that they are enriched in both compatible and incompatible REEs relative to chondorite values. The REE patterns are all characterized by LREE enrichment and by lack of Eu anomaly (Eu_N/Eu^*=0.8–1.16). The absence of negative anomaly in Eu may be due to the high magmatic oxidation states (e.g., Richards *et al*., 2001). High LILE/REE and LILE/HFSE ratios are usually attributed to mass transfer of fluids from the subducted slab in to the overlain mantle wedge and the fluids have led to metasomatism and enrichment of those elements in the sub-arc mantle source (Ishizuka, *et al*; 2003; Vroon *et al*., 1993; Chesly *et al*., 2003).

Some studies of Late Cenozoic volcanic rocks from the central volcanic zone of the Andes have shown that the REE provide powerful indicators of melting depth or fractionation of arc magmas (Kay *et al*., 1991, 1999; Trumbull *et al*., 1999). Below depths of 30-45 km, garnet can be an important residual phase; so, the magma that fractionated at these depths, depleted strongly of HREE (garnet preferentially retains HREE over LREE; Frey *et al*., 1978; Hanson, 1980). In contrast, fractionation of amphibole will result in modest HREE depletions and generation of listric

shaped patterns (hornblende preferentially retains MREE).

All of the studied rock samples show a slight steep pattern with (La/Yb)n values ranging from 3.13 to 17.84, (La/Lu)n values ranging from 1.2 to 16.01 and (Ce/Yb)n values ranging from 1.98 to 10.47. Nd shows a marked positive anomaly and the light rare earth elements (LREE) are variably enriched [i.e. (La/Sm)n=2.57-6.40] relative to those of the HREE [i.e. (Gd/Yb)n=1.37-3.55]. This pattern with enrichment of LREE and lack of negative Eu anomaly indicated that the magmatic differentiation may be controlled by an amphibole fractionation.

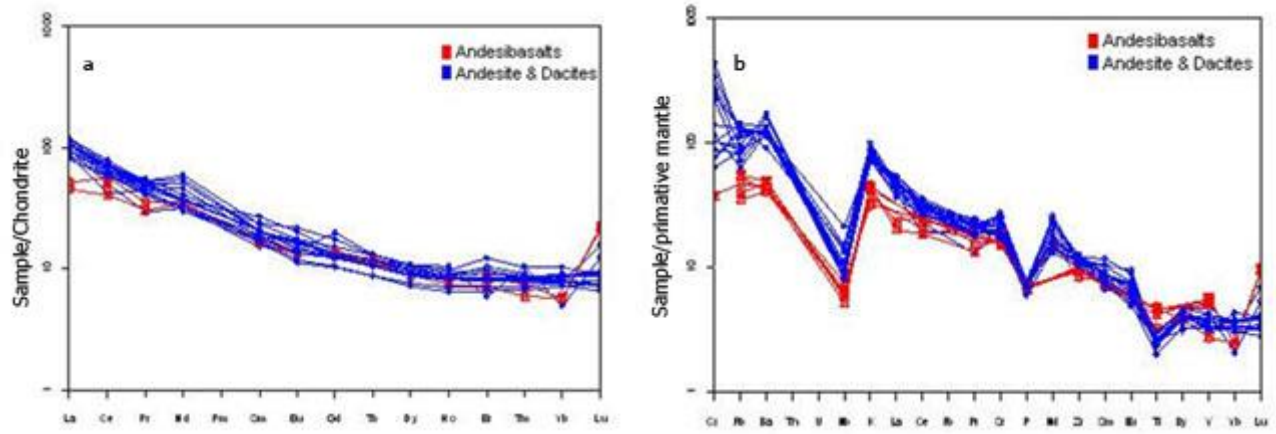

Figure 5 a) Chondrite-normalized rare earth element patterns of volcanic- subvolcanic rocks (chondorite values from Boynton, 1984). b) Primitive mantle-normalized multi-element diagram of the volcanic-subvolcanic rocks (mantle values from Sun and McDonough, 1989).

The Miocene basaltic-andesite lavas are characterized by low La/Sm and La/Yb ratios. These REE patterns and the relatively mafic compositions of these lavas suggest that they experienced limited amounts of fractionation (and assimilation) compared with the intervening andesitic and dacitic magmas and these lavas have preserved the trace element signature of the primary, mantle-derived magma which is input into the arc.

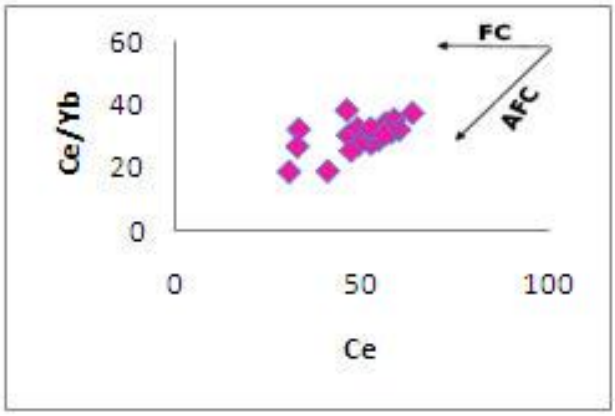

Figure 6) Variation diagram of Ce/Yb versus Ce of the volcanic- subvolcanic rocks (Ajaji et al., 1998).

Besides, Sr and Y decrease with increasing SiO_2 which indicate that fractional crystallization of plagioclase and amphibole could have played an important role during the crystallization of these igneous rocks. These rocks have a single compositional variation in Harker diagrams that suggests a common source for crystallization and evolution of their magma. The transition elements such as Cr, Co, Sc, Ni and V have a negative correlation with their silica content. That is, they behave as compatible elements. These negative anomalies become deeper from basaltic andesite to dacite, which is also characteristic for calc-alkaline arc related evolution. The decrease of V content with an increasing SiO_2 may be an evidence for the fractionation of Fe-Ti oxides. The decreasing trend for Ni (substitute for Fe or Mg in amphibole) is consistent with its compatibility in the early crystallizing minerals, whereas an increasing trend of Rb (substitute for K) is correlative with the late crystallization of biotite and sometimes K-feldspar. As a whole, the

behavior of a number of trace elements with increasing SiO_2 suggests that those variations in the primary composition of the igneous rocks were the result of fractional crystallization.

The Ce/Yb vs. Ce diagram can be used to determine the magmatic processes involved in magma generation (Ajaji *et al*., 1998, Fig. 6). This diagram suggested the role of assimilation and fractional crystallization processes (AFC) for the studied granitoids (especially in andesite to dacite samples). The samples trend corresponds to the AFC processes. Ce and Pb as two highly incompatible elements, have similar separation coefficients in low pressure fractionation conditions (Pearce and Parkinson 1993). These elements show the horizon trend during differentiation but in assimilation process or due to magma mixing show increasing linear trend or curve trend respectively (Fig. 7). So based on this diagram, we can say that assimilation associated with fractional crystallization is responsible for magma evolution simultaneously.

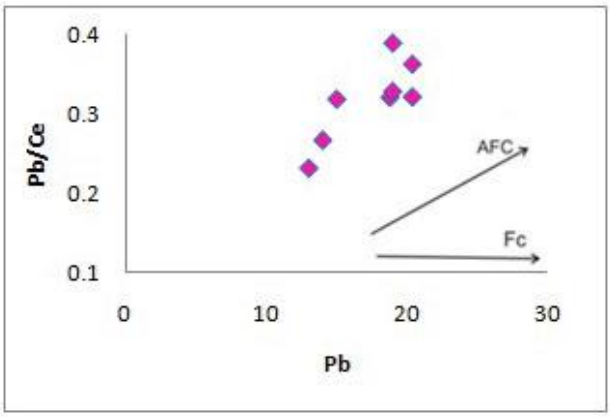

Figure 7) Variation diagram of Pb/Ce versus Pb of the volcanic- subvolcanic rocks show the role of assimilation fractional crystallization for the evolution of magma.

The studied igneous rocks in the geotectonic classification of pearce *et al*. (1984) are classified as volcanic arc granitoids. Furthermore, these granitoids are enriched in LILE such as Cs, K, Rb and Th with respect to the HFSE, especially Nb and Ti. The magmas with these geochemical characters are generally ascribed to subduction environments (e.g., Rogers and Hawkesworh, 1989; Sajona *et al*., 1996).

5.2- Sr-Nd geochemistry

The $^{87}Sr/^{86}Sr$ isotopic ratios have been determined in 24 samples of basaltic andesites to dacites. The $^{143}Nd/^{144}Nd$ isotopic ratios have been identified only in 6 samples. The results are presented in Table 2. $^{87}Sr/^{86}Sr$ and $^{143}Nd/^{144}Nd$ isotopic ratios are from 0.705201 to 0.707187 (Sr_i=0.705229–0.707012) and 0.512508 to 0.512646 respectively. The isotopic ratios of volcanic rocks which are erupted in island arcs and continental margins, plot in 2nd and 4th quarter of the Sr-Nd diagram (Gunter, 1986). All six studiedsamples plotted in the lower right quadrangle of the Sr-Nd diagram (Fig. 8).

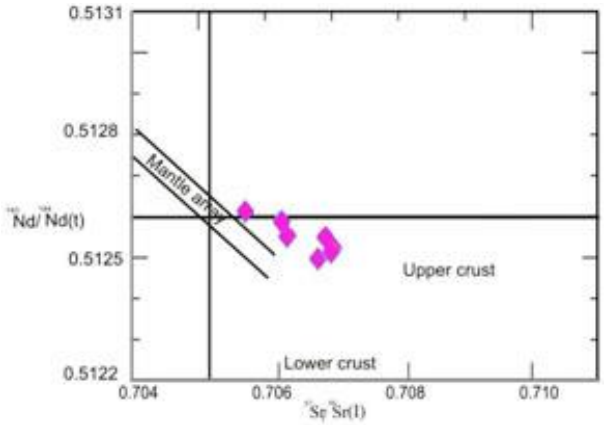

Figure 8) $^{143}Nd/^{144}Ndi$ vs.$^{87}Sr/^{86}Sri$ ratios for Salafchegan granitoid rocks at 25 Ma.

Isotopic ratio of andesitic basalt is close to the mantle array, however isotopic ratios of other samples are located between mantle array and crustal rocks (tend to the upper crust). All of these samples are characterized by negative εNd values (between -0.5 to -2.1) which can show the role of crustal contamination in their petrogenesis. Of course enrichment of lithospheric mantle which is a predictable and important differentiation process beneath orogenic belts and has operated on earth for at least the past 3 billion year (Chiarenzelli *et al*., 2009) should not be ignored. Also this process has been confirmed by some geochemistry evidences such as enrichment of LILE relative

to REE and HFSE and also by negative εNd values. In Figure 8, all isotopic values of samples are plotted close together, a feature which shows a genetic link between these rock types. Similarly, the $^{87}Sr/^{86}Sr$ initial isotopic ratios of andesite and dacite are close together, but show lower values (from 0.70509 to 0.70574) for the basaltic andesites. In Figures 9a and d, the $^{87}Sr/^{86}Sr_i$ and $^{143}Nd/^{144}Nd_i$ ratios have been plotted against SiO_2 content of the volcanic-subvolcanic rocks to evaluate the role of assimilation and fractional crystallization processes and the source characteristics. These rocks show near constant $^{87}Sr/^{86}Sr$ and $^{143}Nd/^{144}Nd$ ratios for a range in SiO_2 content from 58.01 to 63.56 wt%. This feature can be explained probably by fractional crystallization of isotopically homogeneous parent magma.

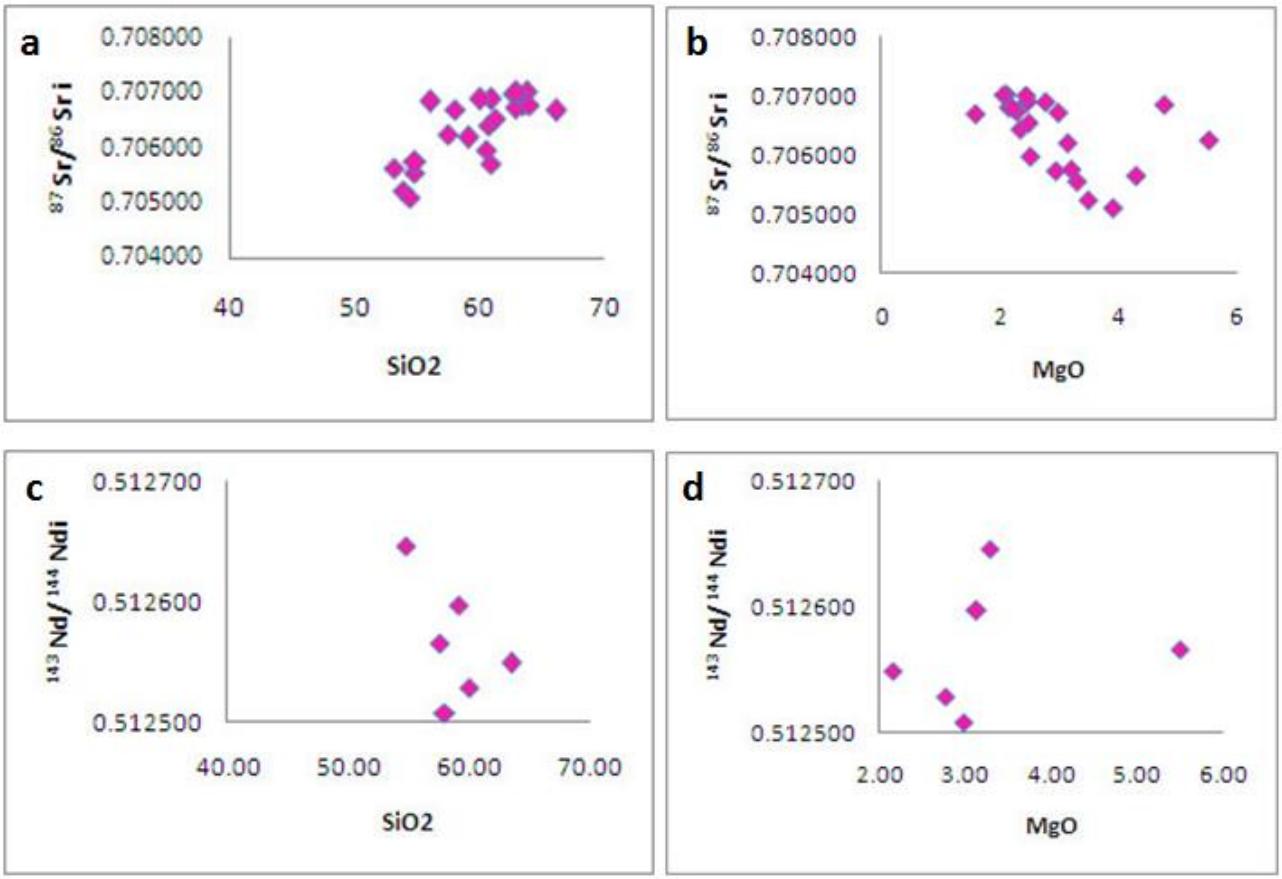

Figure 9) Variation diagrams of $^{87Sr}/^{86}Sri$ (a,b) and $^{143}Nd/^{144}Nd$ ratios (c,d) vs. SiO_2 and MgO.

The $^{87}Sr/^{86}$ Sr ratios of Salafchegan igneous rocks are in approximately positive correlation with SiO_2 but negatively correlated with MgO (Figs. 9a and b). Nd isotopic contents are positively correlated with MgO but negatively correlated with SiO_2 (Figs. 9c and d). These correlations indicate that these rocks are likely formed by a combination of fractional crystallization and crustal contamination. Contamination might occur during the upward motion of the magma through crustal rocks. On the other hand, radiogenic isotope ratios of these rocks are more and less consistent with derivation of their parental magma from a metasomatized subcontinental lithospheric mantle source. Of course understanding of the magma genesis in collision zones is difficult because so many processes are involved, including for example, contamination by fluids, melts and subducted sediments in mantle source and/or contamination of mantle derived magmas by assimilation of lithospheric mantle or crustal rocks during ascent and emplacement (e.g., Davidson, 1996).

Considering all the evidences, it seems that a set of enriched lithospheric mantle (which is required to create andesitic magma from mantle) and crustal assimilation have been

involved in the development of salafchegan granitoids. In Figure 10, a schematic model proposed for the formation of magma and igneous rocks in Salafchegan area.

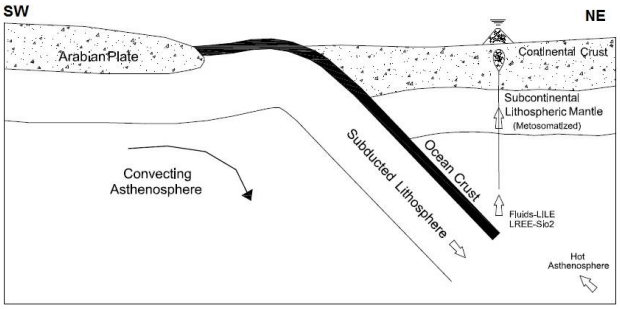

Figure 10) A schematic model of magma and igneous rocks formation in Salafchegan area (without scale).

6- Conclusion

Salafchegan arealies along Urumieh-Dokhtar volcanic belt which comprises of Miocene-Pliocene bodies of basaltic andesite, andesite, dacite, diorite and quartz-diorite with porphyry texture exposing as volcanic and subvolcanic bodies. Geochemical data of the studied igneous rocks, such as LILE enrichment relative to HFSE, negative anomalies of Nb, P and Ti and positive anomaly in Pb, show that parental magma is similar to calc-alkaline magmas related to continental margin arc environment. In this calc-alkaline magma which has abundant amphibole and biotite phenocrysts and therefore has high magmatic water contents, plagioclase crystallization can be postponed until final stages of fractionation. This factor can be the explanation for the lack of Eu anomaly in this system. The relatively low MgO concentration of Salafchegan granitoids and depletion of Fe, Ca, Mg, Sr, Y, Mn and Ni suggests that significant degrees of fractional crystallization of ferromagnesian phases such as hornblende and pyroxene occurred during the formation of these igneous rocks. The LILE enrichment relative to REE and HFSE attributed to mass transfer of fluids from the subducted slab in to the overlain mantle wedge and metasomatism of the sub-arc mantle source by these fluids enriched in these elements.

The normalized REE and trace element patterns have similarity and suggest that all of these rocks evolved from the same source. These interpretations are also supported by radiogenic isotopic ratios. Their narrow isotopic ratios suggest that these rock typesare related to each other genetically.

All isotopic ratios placed in the fourth quarter of the Sr-Nd diagram close to mantle array and upper crustal range. Similarly, all samples are characterized by negative εNd values; reflect the role of crustal contamination.The correlations between isotopic ratios and SiO_2 and MgO prove that combination of fractional crystallization and crustal contamination hasan effective role in the petrogenesis of the Salafchegan igneous rocks. Furthermore, the correlation of increasing Sr ratios with SiO_2 is due to gradual assimilation of radiogenic isotope ratios from crust as the melt differentiates (increasing SiO_2) during ascent through crust. Generally, all of the above evidences suggest that magma responsible for Miocene-Pliocene granitoids in Salafchegan area, were derived from an enriched lithospheric mantle source and were subsequently modified by assimilation and fractional crystallization processes during its ascent.

Acknowledgments:

The author thank Prof. Danielle Demaiffe and Dr. Olivier Féménias of the Université Libre de Bruxelles for their help in doing isotopic analyses and Prof. Fuat yavuz (Istanbul Teknik University), Dr. Julien Berger (Université Paul Sabatier) and Dr Jamshid Ahmadian (Payame Noor University) for their helpful suggestions.

References:

Alavi, M. 1994. Tectonics of the Zagros orogenic belt of Iran: new data and interpretations. Tectonophysics: 220, 211–238.

Ayati, F., Mahdevari, S. 2010. The comparison between hydrothermal and magmatic biotites

in Sakht-Hesar igneous rocks. Journal of Economic Geology: 1(1), 117–134 (in Persian).

Ayati, F., Yavuz, F., Asadi, H., Richards, J., Jourdan, F. 2013. Petrology and geochemistry of calc-alkaline volcanic and subvolcanic rocks, Dalli porphyry copper–gold deposit, Markazi Province, Iran. International Geology Review: 55, 158–184.

Ayati, F., Yavuz, F., Noghreyan, M., Haroni, A., Yavuz, R. 2008. Chemical characteristics and composition of hydrothermal biotite from the Dalli porphyry copper prospect, Arak, central province of Iran. Mineralogy and Petrology: 94, 107–122.

Bologne, G., Duchesne, J. C. 1991. Analyses des roches silicate par spectrometrie de flurescence X: precision et exactitude. Belgium Geology Survey: 249, 1–11.

Boynton, W. V. 1984. Cosmochemistry of the rare earth elements: meteorite studies,in: Henderson, P. (Eds.), Rare Earth Element Geochemistry. Elsevier Science: pp. 63–114.

Burnham, C. W. 1979. Magmas and Hydrothermal fluids, in: Barnes, H.L. (Eds.), Geochemistry of Hydrothermal Ore Deposits. Wiley, New York, pp. 63–123.

Chappel, B. W., White, A. J. R. 1974. Two contrasting granite types. Pacific Geology: 8, 173–174.

Chesley, J., Righter, K., Ruiz, J. 2004. Large-scale mantle metasomatism: A Re-Os perspective. Earth and Planetary Science Letters: 219, 49–60.

Chiarenzelli, J., Lupulescu, M., Cousens, B., Thern, E., Coffin, L., Regan, S. 2009. Enriched Grenvillian lithospheric mantle as a consequence of long-lived subduction beneath Laurentia. Geology: 38, 151–154.

DePaolo, D. J. 1981. Trace element and isotopic effects of combined wall rock assimilation and fractional 387 crystallization. Earth and Planetary Science Letters: 53, 189–202.

Faure, G. 1986. Principles of isotope geology, 2nd edition. John Wiley and Son, New York.

Féménias, O. 2003. Contribution à l'étude du magmatisme tardi- à post-orogénique. De sa source à sa mise en place en sub-surface: exemples régionaux de l'essaim de filons du Motru (Roumanie) et du complexe lité profond sous Beaunit (France). PhD dissertation, Université Libre de Bruxelles.

Geological Survey of Iran, 2000, Salafchegan-Khorhe 1:100,000 geological map, 1 sheet.

Gill, J. B. 1981. Orogenic andesite and plate tectonic. Springer-Verlag, Berlin.

Grove, T. L., Elkins Tanton, L. T., Parman, S. W., Chatterjee, N., Muentener, O., Gaetani, G. A. 2003. Fractional crystallization and mantle melting controls on calc-alkaline differentiation trends. Contributions to Mineralogy and Petrology: 145, 515–533.

Hanson, G. N. 1980. Rare earth elements in petrogenetic studies of igneous systems. Annual Review. Earth and Planetary Science Letters: 8, 371–406.

Haschke, M., Ahmadian, J., Murata, M., McDonald, I. 2010. Copper mineralization prevented by arc-root delamination during Alpine-Himalayan collision in central Iran. Economic Geology: 105, 855–865.

Hawkeswoth, C. J., Hergt, J. M., Ellam, R. M., Mcdermott, F. 1991. Element fluxes associated with subduction related magmatism. Philosophical Transactions of the Royal Society of London: 335, 167–79.

Hawkesworth, C. J., Turner, S. P., McDermott, F., Peate, D. W., Van Calsteren, P. 1997. U–Th isotopes in arc magmas: implications for element transfer from subducted crust. Science: 276, 561–555.

Hezarkhani, A. 2002. Mass change during hydrothermal alteration/mineralization in a porphyry copper deposits, eastern Sungun, northwestern Iran. Journal of Asian Earth Sciences: 28, 423–438.

Ishizuka, O. Taylor, R. N. Milton, J. A, Nesbitt, R. W. 2003. Fluid-mantle interaction in an intra-oceanic arc: constraints from high-precision Pb isotopes. Earth and Planetary Science Letters: 211, 221–236.

Jamali, H., Dilek, Y., Daliran, F., Yaghubpur, A., Mehrabi, B. 2010. Metallogeny and tectonic evolution of the Cenozoic Ahar-Arasbaran volcanic belt, northern Iran. International Geology Review: 52, 608–630.

Kay, R. W., Mahlburg, S. 1991. Creation and destruction of lower continental crust. Geologische Rundschau: 80, 259–278.

Kay, S. M., Mpodozis, C., Coira, B. 1999. Magmatism, tectonism, and mineral deposits of the Central Andes (22°-33°S latitude), in: Skinner, B. (ed.), Geology and Ore Deposits of the Central Andes. Society of Economic

Geology, Special Publication (SEG): 7, 27–59.

Langmuir, C. H., Vocke, R. D., Hanson, G. N., Hart, S. N. 1978. A general mixing equation with applications to Icelandic basalts. Earth and Planetary Science Letters: 37, 380–92.

Mohajjel, M., Fergusson, C. L., Sahandi, M. R. 2003. Cretaceous-Tertiary convergence and continental collision, Sanandaj-Sirjan zone, western Iran. Journal of Asian Earth Sciences: 21, 397–412.

Pearce, J. A., Peate, D. W. 1995. Tectonic implications of the composition of volcanic arc magmas. Annual Review. Earth and Planetary Science Letters: 23, 251–285.

Pearce, J. A., Harris, N. B. V., Tindle, A. G. 1984. Trace element discrimination diagrams for the tectonic interpretation of granitic rocks. Journal of Petrology: 25, 956–983.

Pearce, J. A. 1982. Trace element characteristics of lavas from destructive plate boundaries, in: Gill, J. (Eds.), Andesites: orogenic andesites and related rocks. John Wiley and Sons, Chichester, U.K., pp.525–548.

Peccerillo, A., Taylor, S. R. 1976. Geochemistry of Eocene calc-alkaline volcanic rocks from the Kastamonu area, Northern Turkey. Contributions to Mineralogy and Petrology: 58, 63–81.

Pei, R. F., Hong, D. W. 1995. The granites of South China and their metallogeny. Episodes: 18, 77–86.

Pourhosseini, F. 1982. Petrogenesis of Iranian plutons: a study of the Natanz and Bazman intrusive complexes. PhD Thesis,University of Cambridge.

Richards, J. P., Boyce, A. J., Pringle, M. S. 2001. Geologic evolution of the Escondida area, northern Chile: A model and temporal localization of porphyry Cu mineralization. Economic Geology: 96, 271–305.

Rogers, G., Hawkesworth, C. 1989. A geochemical traverse across the North Chilean Andes: Evidence for crust generation from the mantle wedge. Earth and Planetary Science Letters: 91, 171–185.

Sajona F. G., Maury, R. C., Bellon, H., Cotton, J. Deffand, M. 1996. High field strength elements enrichment of Pliocene-Pleistocene Island arc basalts, Zammbuanga Peninsula, western Mindanao. Journal of Petrology: 37, 693–726.

Sokoutis, D., Bonini, M., Medvedev, S., Boccaletti, M., Talbot, C., Koyi, H. 2000. Indentation of a continent with a built-in thickness change: experiment and nature. Tectonophysics: 320, 243–270.

Sun, S., McDonough, W. F. 1989. Chemical and isotopic systematic of oceanic basalts: implications for mantle composition and processes. In: Saunders, A. D., Norry, M. J. (Eds.), Magmatism in the Ocean Basins. Geological Society Special Publication 42, Oxford, Blackwell Scientific Publications, pp.313–345.

Trumbull, R., Wittenbrink, R., Hahne, K. 1999. Evidence for late Miocene to recent contamination of arc andesites by crustal melts in the Chilean Andes (25–26) and its geodynamic implications. Journal of South American Earth Sciences: 12, 135–155.

Vander Auwera, J., Bologne, G., Roelants, I., Duchesne, J. C. 1998. Inductively coupled plasma-mass spectrometric analysis of silicate rocks and minerals. Geology Belgium: 1, 49–53.

Voshage, H., Hofmann, A. W., Mazzucchelli, M., Rivalenti, G.,Sinigol, S.,Raczek, I., Demarchi, G.1990. Isotopic evidence from the Ivrea zone for a hybrid lower crust formed by magmatic underplating. Nature: 347, 731–6.

Vroon, P. Z, Bergen, M. J. V, White, W. M, Varekamp J. C. 1993. Sr-Nd-Pb isotope systematics of the Banda arc, Indonesia: combined subduction and assimilation of continental material. Journal of Geophysical Research: 98, 22349–22366.

Vroon, P. Z., Van Bergen, M. J., White, W. M., Varekamp, J. C. 1993. Sr–Nd–Pb isotope systematic of the Banda Arc, Indonesia: combined subduction and assimilation of continental material. Journal of Geophysical Research: 98, 22349–66.

Wang, Q., Xu, J. F., Jian, P., Bao, Z. W., Zhao, Z. H., Li, C. F., Xiong, X. L., Ma, J. L. 2006. Petrogenesis of Adakitic Porphyries in an Extensional Tectonic Setting, Dexing, South China: Implications for the Genesis of Porphyry Copper Mineralization. Journal of Petrology: 47, 119–144.

Whitney, J. A. 1975. The effects of pressure, temperature and xH2O on phase assemblages

in four synthetic rock compositions. Journal of Geology: 83, 1–32.

Whitney, J. A., Stormer, J. C. 1985. Mineralogy, petrology and magmatic conditions of the Fish Canyon Tuff, Central San Juan volcanic field, Colorado. Journal of Petrology: 26, 726–762.

Zarasvandi, S., Liaghat, S., Zentilli, M. 2005. Geology of the Darreh-Zerreshk and Ali-Abad porphyry copper deposits, central Iran. International Geology Review: 47, 620–646.

Zindler A., Hart, S. 1986. Chemical geodynamics. Annual Review of Earth and Planetary Sciences: 14, 493–571.

Zhou J. X. 1999. Geochemistry and Petrogenesis of Igneous Rocks Containing Amphibole and Mica: A Case Study of Plate Collision Involving Scotland and Himalayas. New York and Beijing Science Press: 41–72.